

Strain-induced structural phase transition of a Ni lattice through dissolving Ta solute atoms

Q. Zhang, W. S. Lai, and B. X. Liu*

Advanced Materials Laboratory, Department of Materials Science and Engineering, Tsinghua University, Beijing 100084, China

(Received 24 August 2000; revised manuscript received 30 January 2001; published 7 May 2001)

The structural phase transition of a single-crystal Ni lattice upon dissolving Ta solute atoms is investigated by means of molecular-dynamics simulations with a realistic n -body Ni-Ta potential. It is found that when the solute concentration is within 9–19 at. % of Ta, the accumulated strain results in a martensitic phase transition, i.e., face-centered-cubic (fcc) Ni transforms into a face-centered-orthorhombic-(fco) like structure through shearing, and that when the solute concentration is over 21 at. % of Ta, the Ni lattice collapses and turns into an amorphous state. Comparatively, for the case of an initial hcp Ni lattice, the same martensitic and amorphization transitions also take place. The former hcp-fco transition, however, is mainly through atomic rearrangement as well as readjustment of lattice parameters, and the resultant state is almost perfect single crystal with no shearing bands. Besides, the above structural transitions are frequently in association with a dramatic softening in shear elastic moduli.

DOI: 10.1103/PhysRevB.63.212102

PACS number(s): 61.43.Dq, 62.20.Fe, 64.70.Pf, 68.35.Rh

Since the early 1980s, several techniques, such as ion mixing (IM), solid-state interfacial reaction (SSIR), and mechanical alloying (MA), have emerged and produced a great number of metastable alloys with either an amorphous or a crystalline structure in the binary metal systems.^{1–3} To understand the underlying mechanism responsible for the crystal-to-amorphous transition, molecular dynamics (MD) simulations have proved to be a powerful method to trace the structural evolution that results in the formation of the metastable alloys.^{4–8} To the authors' knowledge, most of the simulation studies were concentrated on the crystal-to-amorphous transition, whereas only a few simulations concerning the crystal-to-crystal transition have so far been reported. In our previous MD simulation study of the Ni-Ta system, we focused on the crystal-to-amorphous transition by tracing solid solutions with increasing solute concentration, yet the structural evolution of the solid solutions before spontaneous decay was not studied in detail.⁸ It is known that the time scale involved in the simulation is far below 1 s, which is much too short for a crystalline structure to nucleate and grow. On the contrary, if the growth of a specific crystalline phase proceeds by a fast transition process, e.g., through a martensite transformation, MD simulations are able to reveal the associated transition mechanism at an atomic scale. We report, in this paper, MD simulation results concerning structural evolution in the single-crystal Ni lattice upon dissolving the Ta solute atoms, which results in a crystal-to-crystal transition before spontaneous decay.

MD simulations are carried out with a Parrinello-Rahman constant-pressure scheme,⁹ and the equations of motion are solved using a fourth-order predictor-corrector algorithm of Gear with a time step $t = 5 \times 10^{-15}$ s. In the simulation, the interactions between atoms are described with an n -body potential.⁸

A fcc Ni single-crystal model is first constructed to consist of $8 \times 8 \times 8 \times 4 = 2048$ atoms. In the model, three axes A , B , and C of the computational box corresponding to the $[100]$, $[010]$, and $[001]$ crystalline directions, respectively, are set to be parallel to x , y , and z directions, and periodic boundary conditions are adopted. Second, a certain amount

of Ni atoms in the fcc lattice are randomly selected and substituted by the Ta solute atoms to form a fcc Ni-rich solid solution. The solid solution model is then run at a constant temperature 300 K to reach a relatively equilibrium state, at which all dynamic parameters show no secular variation.

To characterize the resultant structure after equilibrating, the radial distribution functions $g(r)$ are calculated and shown in Fig. 1. It can be seen that when the concentration

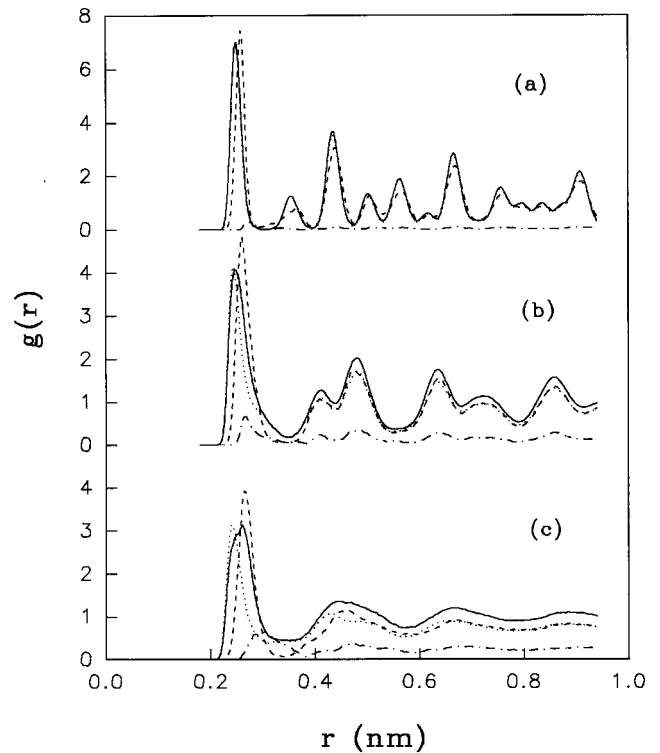


FIG. 1. Total and partial pair-correlation functions for fcc Ni-rich solid solutions after running at 300 K. The compositions are of (a) 5 at. %, (b) 15 at. %, and (c) 25 at. % of Ta, respectively. The solid line is for total $g(r)$, the short dashed line is for Ta-Ni $g(r)$, the dotted line is for Ni-Ni $g(r)$, and the dot-dashed line is for Ta-Ta $g(r)$.

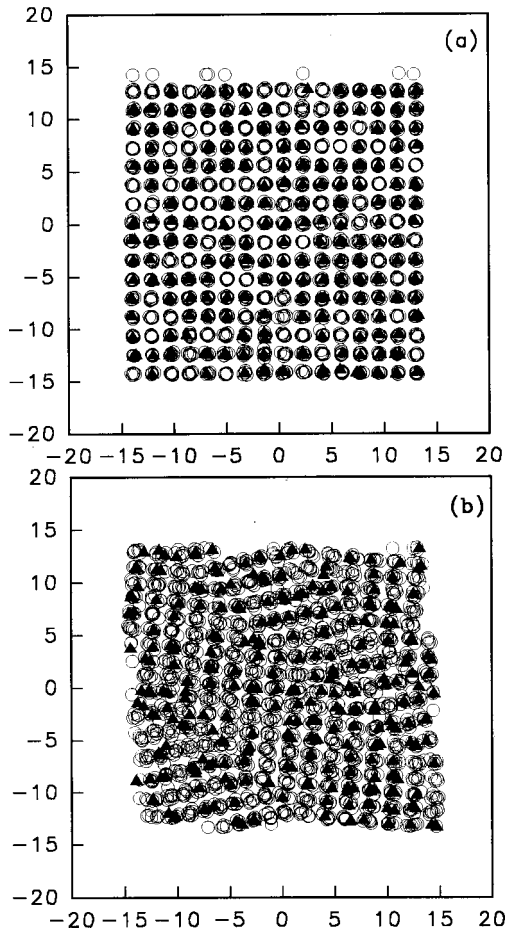


FIG. 2. The projections of the atomic positions of fcc Ni-rich solid solutions with Ta concentrations of (a) 5 at. % and (b) 15 at. %, respectively, after equilibrating at 300 K. Open circle: Ni. Solid triangle: Ta.

of the Ta solute atoms is less than 8 at. %, the fcc crystalline structure is preserved and that when the Ta concentration is between 9 and 20 at. %, the fcc lattice turns into a face-centered-orthorhombic- (fco-) like structure. Further increasing the Ta concentration up to 21 at. %, the corresponding $g(r)$ features a shape commonly known as an amorphous structure, indicating that the initial fcc lattice has turned into an amorphous state. The variation of the computational box of fcc Ni solid solutions with different solute concentrations

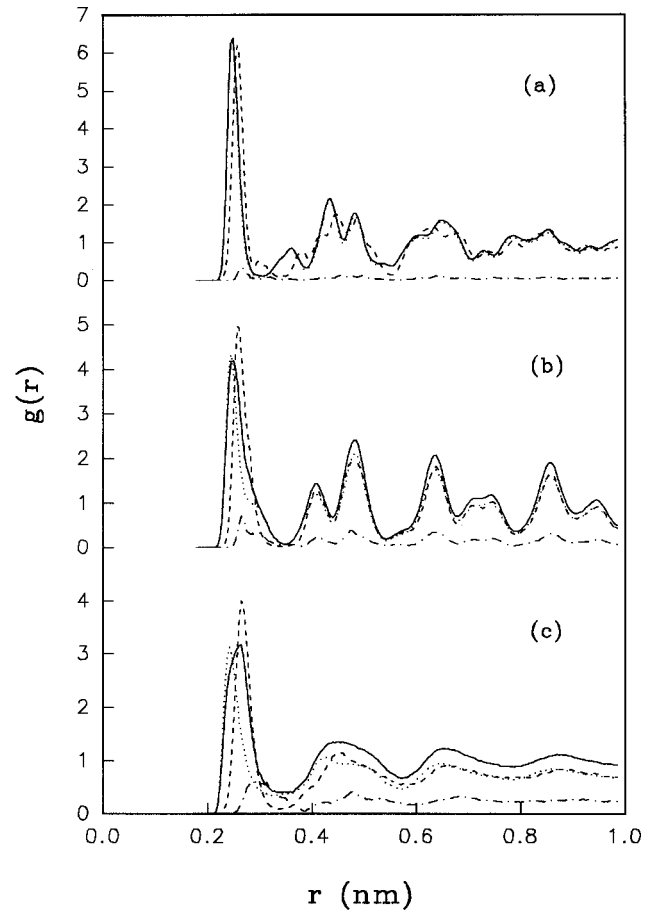


FIG. 3. Total and partial pair-correlation functions for hcp Ni-rich solid solutions after running at 300 K. The Ta concentrations are of (a) 5 at. %, (b) 15 at. %, and (c) 25 at. %, respectively. The solid line is for total $g(r)$, the short dashed line is for Ta-Ni $g(r)$, the dotted line is for Ni-Ni $g(r)$, and the dot-dashed line is for Ta-Ta $g(r)$.

is given in Table I. One observes that after dissolving 8 at. % Ta the Ni lattice remains almost cubic, the same as fcc Ni single crystal, except for the increase of the length of the box from approximately 2.8 nm of Ni single crystal to 2.9 nm of Ni solid solution. This suggests that the Ni solid solution with 8 at. % Ta still retains fcc structure, which is the same as that of 5 at. % Ta shown in Fig. 1(a). Interestingly, it can be seen that when the solute concentration is of 15 at. % Ta

TABLE I. Variation of the computational box of fcc Ni solid solutions with different solute concentrations after simulations performed at 300 K for 0.1 ns. Here A , B , and C are three axes of the computational box, and α , β , and γ are the corresponding angles of these axes: i.e., α is an angle between the axes B and C , β an angle between the axes C and A , and γ an angle between the axes A and B .

Composition (at. % Ta)	A (nm)	B (nm)	C (nm)	α (deg)	β (deg)	γ (deg)
0	2.828	2.832	2.828	89.981	90	90.007
8	2.865	2.871	2.899	89.971	90.194	90.038
15	2.872	2.666	3.246	89.54	90.631	92.595
25	2.947	2.920	2.986	89.834	90.23	89.594

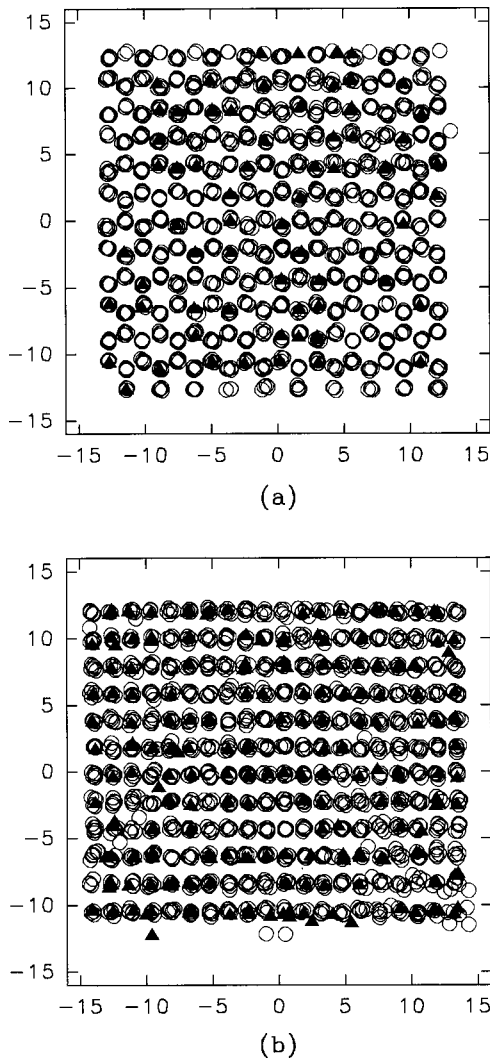


FIG. 4. The projections on a plane perpendicular to the C axis of the atomic positions of hcp Ni-rich solid solutions with Ta concentrations of (a) 5 at. % and (b) 15 at. %, respectively, after equilibrating at 300 K. Open circle: Ni. Solid triangle: Ta.

three edges of the computational box vary asymmetrically; i.e., after equilibrating at 300 K for 0.1 ns, the edges for the original as-set model of 2.816 nm in all three directions change into 2.872, 2.666, and 3.246 nm, respectively. Moreover, the angles α and β still keep almost 90° , whereas γ increases from 90° to 92.595° . In other words, the dimension of the B axis is reduced, while the other two dimensions of the A and C axes are both elongated, implying that a structural transition takes place in the Ni lattice after dissolving 15 at. % Ta solute atoms.

Some interesting features are observed after the above structural transition for the fcc Ni-rich solid solutions with solute concentration of 9–20 at. % Ta. It is found that some coherent shear bands are produced in the crystal and that the initial fcc single crystal changes into a fco-like structure. To illustrate the effect of the Ta solute atoms on the resultant structure, Fig. 2 shows a projection of the atomic positions of a Ni-rich solid solution with 15 at. % of Ta after equilibrating at 300 K to compare with that of a Ni-Ta (5 at. %) fcc solid

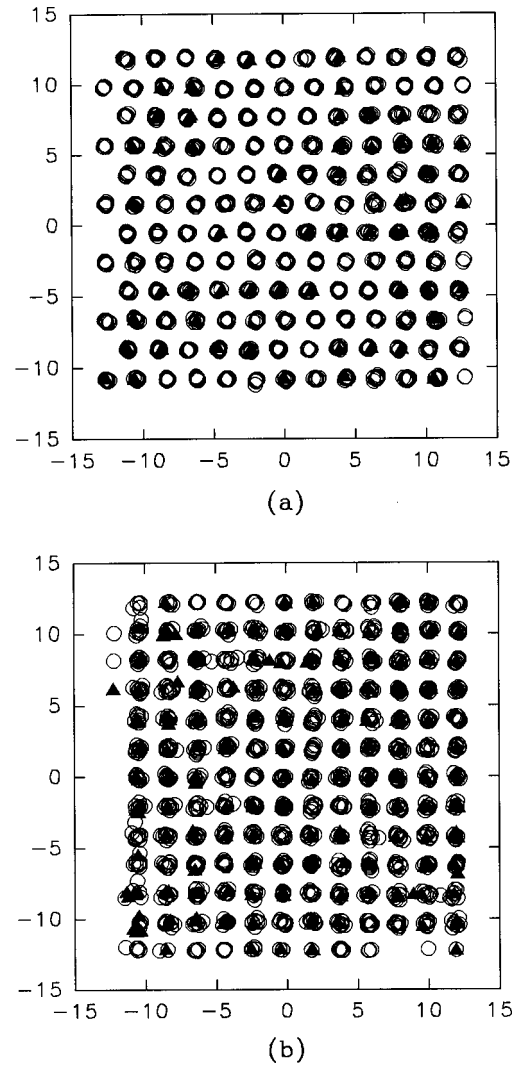


FIG. 5. The projections on a plane perpendicular to the A axis of the atomic positions of hcp Ni-rich solid solutions with Ta concentrations of (a) 5 at. % and (b) 15 at. %, respectively, after equilibrating at 300 K. Open circle: Ni. Solid triangle: Ta.

solution, from which the sheared regions can vividly be seen. In fact, the shear events are in cooperative with different changes in the lattice dimensions. In the case of Ni-rich solid solution with 15 at. % Ta, as shown in Table I, the dimension of the B axis is reduced, while the other two dimensions of the A and C axes are both elongated. The configuration of the shear bands shown in Fig. 2 is a projection on a plane perpendicular to the most elongated C axis. It is also noted that in the other two directions along the A and B axes no reorientation is observed, and the original crystalline planes perpendicular to the C axis can still be distinguishable, suggesting that the shear events occur along the direction perpendicular to the most elongated C axis. Referring again to Fig. 2, one notices that there are shear events occurring on the (110) plane. This is probably the reason responsible for the increase of the γ angle mentioned above. Furthermore, simulation results reveal that the elongation or strain of the lattice takes place at the first 0.02–0.03 ns and the strain rates are calculated to be $(0.45\text{--}0.65)\% \text{ ps}^{-1}$. These results

are quite compatible with a recent report that the cooperative shear events (twins) could take place in a perfect crystal upon application of strain at a rate of $0.5\% \text{ ps}^{-1}$ and less.¹⁰ In comparison, for the Ni-Ta solid solution models where amorphization takes place, lattice elongation is observed in three directions: e.g., for a solid solution of 25 at. % Ta, as given in Table I, they are elongated to about 2.95 nm. It is also true for the solid solution models with Ta solute atoms less than 9 at. %: e.g., for 8 at. % of Ta the lengths are all elongated to about 2.87 nm.

It is known that the fcc and hcp structures are very much alike and their cohesive energies are indeed calculated to be quite close based an n -body Ni-Ta potential.⁸ We therefore also perform a MD simulation for a single-crystal hcp Ni lattice consisting of $10 \times 6 \times 6 \times 4 = 1440$ atoms to find out if some new features would emerge in the structural evolution. In the model, the axes A , B , and C of the computational box corresponding to $[2110]$, $[0110]$, and $[0001]$ crystalline directions are set to be parallel to the x , y , and z axes, respectively, and periodic boundary conditions are also adopted. Similarly, the Ni atoms in the hcp lattice are randomly selected and substituted by the Ta solute atoms, and the model is then run at a constant temperature 300 K to reach a relatively equilibrium state.

The radial distribution functions $g(r)$ are calculated for the resultant structures, and Fig. 3 exhibits the calculated curves for the hcp Ni-rich solid solutions with 5, 15, and 25 at. % of Ta. It can be seen that when the Ta solute is of 5 at. %, i.e., less than 8 at. %, the hcp crystalline phase is preserved, and that when the Ta solute is of 15 at. %, i.e., between 9 and 20 at. %, the radial distribution functions are similar to those shown in Fig. 1(b), suggesting that no matter what the initial Ni lattice is, by dissolving Ta solute atoms within 9–20 at. % the resultant structure is the same. Further increasing the Ta concentration up to 25 at. %, i.e., greater

than 21 at. %, an amorphous structure is obtained. Figures 4 and 5 show the projections of the atomic positions of the resultant structures transformed from the hcp Ni-rich solid solutions with 5 and 15 at. % of Ta on two planes perpendicular to the C and A axes, respectively. It is of interest to notice that unlike the structural transition beginning with a fcc Ni lattice, the transition from the hcp Ni lattice has no shear bands, and the resultant structure is almost a perfect lattice. Moreover, the axes of the computational box for Ni-rich solid solutions with 5 and 15 at. % of Ta are still perpendicular to each other after equilibrating at 300 K. It is seen from Fig. 5 that for a hcp Ni lattice, by dissolving 5 at. % Ta, the hcp structure still remains as the atomic stacking sequence along the C axis is observed to be $ABAB\dots$, while such a sequence no longer remains for the hcp Ni lattice after dissolving 15 at. % Ta. The resultant state for the latter case is face-centered-orthorhombic structure. The hcp-fcc transition is realized through atomic rearrangement as well as readjustment of the lattice parameters.

In summary, the above simulation results indicate that dissolving Ta solute atoms into a Ni fcc or hcp single-crystalline lattice can induce considerable stress in the lattice. If the stress is small, the fcc lattice can relax the stress through a volume expansion. When the stress reaches a medium level, the initial crystalline lattice transforms into a reoriented fcc crystal through a heterogeneous plastic deformation and the fcc crystal contains some cooperatively sheared regions. Further increasing the stress up to a high level, which cannot be accommodated through a strain relaxation, the initial crystal lattice turns into a disordered state. Similar structural evolution also takes place in the hcp Ni-rich solid solution, yet the hcp-fcc structural transition is realized through atomic rearrangement with no sheared bands appearing.

*Corresponding author. Electronic address:
dmslbx@tsinghua.edu.cn

¹B. X. Liu, W. L. Johnson, M-A. Nicolet, and S. S. Lau, *Appl. Phys. Lett.* **42**, 45 (1983).

²R. B. Schwarz and W. L. Johnson, *Phys. Rev. Lett.* **51**, 415 (1983).

³L. Schulz and J. Eckert, *Topics in Applied Physics* (Springer-Verlag, Berlin, 1994), Vol. 72, Chap. 3.

⁴M. Li and W. L. Johnson, *Phys. Rev. Lett.* **70**, 1120 (1993).

⁵Q. Zhang, W. S. Lai, and B. X. Liu, *Phys. Rev. B* **58**, 14 020

(1998).

⁶R. Devanathan, N. Q. Lam, P. R. Okamoto, and M. Meshii, *Phys. Rev. B* **48**, 42 (1993).

⁷C. Massobrio, V. Pontikis, and G. Martin, *Phys. Rev. B* **41**, 10 486 (1990).

⁸Q. Zhang, W. S. Lai, and B. X. Liu, *Phys. Rev. B* **61**, 9345 (2000).

⁹M. Parrinello and A. Rahman, *J. Appl. Phys.* **52**, 7182 (1981).

¹⁰H. Ikeda, Y. Qi, T. Cagin, K. Samwer, W. L. Johnson, and W. A. Goddard III, *Phys. Rev. Lett.* **82**, 2900 (1999).